2022 IEEE International Conference on Robotics and Automation (ICRA)
May 23-27, 2022. Philadelphia, PA, USA

$\mathcal{L}_1$ Adaptive Augmentation for Geometric Tracking Control of Quadrotors

Zhuohuan Wu, Sheng Cheng, Kasey A. Ackerman, Aditya Gahlawat, Arun Lakshmanan, Pan Zhao and Naira Hovakimyan

2022 IEEE International Conference on Robotics and Automation (ICRA) | 978-1-7281-9681-7/22/$31.00 ©2022 IEEE | DOI: 10.1109/ICRA46639.2022.9811946

Abstract— **This paper introduces an $\mathcal{L}_1$ adaptive control augmentation for geometric tracking control of quadrotors. In the proposed design, the $\mathcal{L}_1$ augmentation handles nonlinear (time- and state-dependent) uncertainties in the quadrotor dynamics without assuming or enforcing parametric structures, while the baseline geometric controller achieves stabilization of the known nonlinear model of the system dynamics. The $\mathcal{L}_1$ augmentation applies to both the rotational and the translational dynamics. Experimental results demonstrate that the augmented geometric controller shows consistent and (on average five times) smaller trajectory tracking errors compared with the geometric controller alone when tested for different trajectories and under various types of uncertainties/disturbances.**

SUPPLEMENTARY MATERIAL

Video: https://youtu.be/25Z7iAkZ5xw
Code: https://github.com/HovakimyanResearch/L1-Mambo

I. INTRODUCTION

In recent years, unmanned aerial vehicles have seen an increased use across a wide range of applications, e.g., surveillance [1], search and rescue [2], agriculture [3], and logistics [4]. The quadrotor platform, in particular, has garnered interests due to its low-cost, relatively simple mechanical structure, and dynamic capabilities [5]–[10]. Controller synthesis for quadrotors is a challenging problem due to the unstable and underactuated nature of the dynamics. The challenges are exacerbated further due to uncertainties and disturbances, potentially leading to a loss of predictability and even stability.

Related Work: Control theoretic methodologies like robust and adaptive control are used to safely operate systems subject to uncertainties. Therefore, such methodologies have been applied for quadrotor trajectory tracking in the presence of uncertainties, e.g., see the survey [11]. However, the synthesis of such controllers relies on simplifying assumptions like linear known (nominal) models and a priori known structured parametric uncertainties that can lead to overly conservative operation. For example, adaptive controllers designed in [12], [13] utilize linearized dynamics. Since the linear models are only valid around the hover-position, the quadrotor cannot track aggressive trajectories. To account for the nonlinear nature of the dynamics, the authors of [14], [15] propose adaptive controllers that use the nonlinear dynamics of the quadrotor. However, the adaptive schemes are developed under the assumption of static/constant uncertainties—an assumption that does not reflect the true time-varying and state-dependent nature of the uncertainties. Other approaches relying on backstepping and sliding-mode techniques have also been developed, e.g., [16]. However, the switching nature of the sliding-mode control causes chattering problems that may excite high-frequency unmodelled dynamics. The chattering behavior is addressed in [17], where the controller is based on Euler angles that suffer from singularities preventing aggressive rotational maneuvers. Disturbance observer-based methods, presented in [18], [19], require decoupled quadrotor dynamics in roll, pitch, and yaw (i.e., diagonal inertia matrix) and can only handle time-dependent and parametric uncertainties. A geometric adaptive tracking controller is presented in [20], where the controller is developed directly on $SE(3)$; however, it assumes an a priori known structure of parametric uncertainties.

Machine learning (ML) tools like deep neural networks (DNNs) and Gaussian process regression (GPR) can accurately learn functions using only the input-output data and do not require any a priori knowledge of the parametric structure. Thus, ML-based control methodologies have been investigated in the literature for quadrotors. In [21], the authors use a DNN to learn the high-order multi-vehicle aerodynamic effects. A tracking controller uses the learned model and is demonstrated in experiments for a quadrotor swarm with individual agents operating in close proximity to each other. In [22], a learning-based model predictive control (MPC) method is proposed, which uses linearized quadrotor dynamics. The authors of [23] model aerodynamic effects using GPR, which are then used by an MPC algorithm to achieve improved tracking performance for high-velocity quadrotor operation. Although ML-based methods can accurately approximate the unmodelled factors, the quadrotor dynamics or the flying environment can significantly change during operation. For example, uncertainties can appear in the form of wind, payload sloshing, and degradation of system capabilities. ML-based methods might fail to react to such changes when these changes are far beyond the scenarios represented in the training datasets. Therefore, ML tools have recently been incorporated within adaptive control to empower them with more agility and flexibility. For example, the work in [24] presents a deep model reference adaptive control architecture. The uncertainties are represented by a

*This work is supported by National Aeronautics and Space Administration (NASA), Air Force Office of Scientific Research (AFOSR), National Science Foundation (NSF) Cyber Physical Systems (CPS) award # 1932529, NSF National Robotics Initiative 2.0 (NRI-2.0) award # 1830639, and NSF-AoF Robust Intelligence award # 2133656.

Mechanical Science and Engineering, University of Illinois Urbana-Champaign, USA. {zw24, chengs, kaacker2, gahlawat, lakshma2, panzhao2, nhovakim}@illinois.edu

DNN, where the inner layers are updated slowly using the collected data. In contrast, the final layer is updated in real-time in an adaptive scheme that uses the inner layers to parameterize the uncertainty. However, the work is focused on the linearized model at the hover position, preventing its applicability to aggressive trajectories.

In light of the considerations mentioned above, we propose a control scheme for quadrotors that uses the $\mathcal{L}_1$ adaptive control as an augmentation to compensate for the nonlinear uncertainties. The use of $\mathcal{L}_1$ adaptive control is motivated by its capability of compensating for uncertainties at an arbitrarily high rate of adaptation limited only by the hardware capabilities [25]. A critical property of the $\mathcal{L}_1$ control enabling the fast adaptation is that the estimation is decoupled from control; thus, the arbitrarily fast adaptation does not destroy the robustness of the closed-loop system [25]. The $\mathcal{L}_1$ adaptive control has been successfully validated on NASA's AirStar 5.5% subscale generic transport aircraft model [26], [27], Calspan's Learjet [28], [29], and unmanned aerial vehicles [30]–[32]. The $\mathcal{L}_1$ adaptive controller design for quadrotors has been studied in [33], [34], where Euler angles are used to model the dynamics. In [35], the authors proposed an $\mathcal{L}_1$ adaptive control augmentation of the geometric controller to avoid the singularities in Euler-angle representation. However, this $\mathcal{L}_1$ augmentation only applies to rotational dynamics, which cannot compensate for any uncertainties in the translational dynamics. Furthermore, the adaptive scheme we propose does not rely on projection and gradient-based optimization, which can potentially cause numerical issues for implementation on the quadrotor in the presence of large adaptation gains [36]. Instead, we use a piecewise-constant adaption law that requires minimal computation [25]. We present an approach that augments a geometric controller with an $\mathcal{L}_1$ adaptive controller for both rotational and translational dynamics. The geometric controller ensures exponential stability for trajectory tracking using the nominal dynamics [10]. Simultaneously, the $\mathcal{L}_1$ adaptive augmentation compensates for non-parametric uncertainties (both state- and time-dependent) and provides guarantees for transient performance and robustness. An initial proof of concept, in simulation, of using $\mathcal{L}_1$ controller for control of a quadrotor can be found in [37]. We demonstrate and validate the proposed architecture through multiple experiments performed on a real quadrotor platform. The results show the $\mathcal{L}_1$ augmentation's superior tracking performance (five times smaller tracking error on average) compared with the geometric controller alone for different trajectories and under various types of disturbances and uncertainties.

Statement of Contributions: i) we provide a new architecture for $\mathcal{L}_1$ control augmentation of a geometric controller for both the rotational and translational dynamics that can compensate for both time- and state-dependent uncertainties; ii) the controller is designed for ease of implementation by formulating the augmentation in the Euclidean space, and by using a piecewise-constant adaptation law that requires minimal computational resources; iii) we test and validate the control scheme empirically on a real quadrotor platform subject to various uncertainties/disturbances and tasked with following different trajectories.

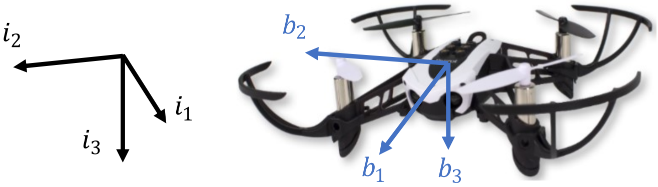

Fig. 1: The Mambo quadrotor and reference frames.

The remainder of the paper is organized as follows: Section II reviews the quadrotor dynamics and the geometric controller design. Section III introduces the $\mathcal{L}_1$ adaptive augmentation of the geometric controller. Section IV shows the experimental results on a Mambo quadrotor. Finally, Section V summarizes the paper and discusses future work.

II. Quadrotor dynamics and geometric controller

We choose an inertial frame and a body-fixed frame, which are spanned by unit vectors $\{i_1, i_2, i_3\}$ and $\{b_1, b_2, b_3\}$ in north-east-down directions, respectively, shown in Fig. 1. The origin of the body-fixed frame is located at the center of mass (COM) of the quadrotor, which is assumed to be its geometric center due to its symmetric mechanical configuration.

The configuration space of the quadrotor is defined by the location of its COM and the attitude with respect to the inertial frame, i.e., the configuration manifold is the special Euclidean group $SE(3)$: the Cartesian product of $\mathbb{R}^3$ and the special orthogonal group $SO(3) = \{R \in \mathbb{R}^{3\times 3} | R^\top R = I,\ \det(R) = 1\}$. By the definition of the rotation matrix $R \in SO(3)$, the direction of the ith body-fixed axis b_i is given by Re_i in the inertial frame, where e_i is the unit vector with the ith element being 1 for $i \in \{1, 2, 3\}$. The rotation matrix can be obtained through the Euler angles yaw ψ, roll ϕ, and pitch θ in the 3-2-1 rotation sequence [38].

The equations of motion of a quadrotor [10] are

$$\dot{p} = v, \tag{1a}$$

$$\dot{v} = ge_3 - \frac{f}{m} Re_3, \tag{1b}$$

$$\dot{R} = R\Omega^\wedge, \tag{1c}$$

$$\dot{\Omega} = J^{-1}(M - \Omega \times J\Omega), \tag{1d}$$

where $p \in \mathbb{R}^3$ and $v \in \mathbb{R}^3$ are the position and velocity of the quadrotor's COM in the inertial frame, respectively, $\Omega \in \mathbb{R}^3$ is the angular velocity in the body-fixed frame, g is the gravitational acceleration, m is the vehicle mass, $J \in \mathbb{R}^{3\times 3}$ is the moment of inertia matrix calculated in the body-fixed frame, f is the collective thrust, and $M \in \mathbb{R}^3$ is the moment in the body-fixed frame. The *wedge* operator $\cdot^\wedge : \mathbb{R}^3 \to \mathfrak{so}(3)$ denotes the mapping to the space of skew-symmetric matrices. Note that we suppress temporal dependencies to maintain clarity of exposition unless required.

We use (1) as the nominal dynamics of the quadrotor to design the geometric controller. Uncertainties in the dynamics will be introduced when we discuss the $\mathcal{L}_1$ adaptive control augmentation in Section III. We do not consider the motor dynamics and the propellers' aerodynamic effects. Therefore, the thrust f and moment M are assumed to be linear in the squared motor speeds [9]. We choose f and M as the control in (1), and they are achieved using the desired motor speeds (see [9] for details in computation).

The design of the geometric controller follows [9], [10], where the goal is to have the quadrotor follow prescribed trajectory $p_d(t) \in \mathbb{R}^3$ and yaw $\psi_d(t)$ for time t in a prescribed interval $[0, t_f]$. The quadrotor dynamics with inputs f and M is differentially flat with flat outputs p_d and ψ_d [9], meaning that the state and inputs of system (1) can be expressed in terms of the flat outputs and their derivatives [39, Sec. 2]. Therefore, the underactuated quadrotor can follow a smooth trajectory in the space of flat outputs $\{p_d, \psi_d\}$.

Define the position and velocity error as $e_p = p - p_d$ and $e_v = \dot{p} - \dot{p}_d$, respectively. We compute the vector of desired force $F_d \in \mathbb{R}^3$ by $F_d = -K_p e_p - K_v e_v - mge_3 + m\ddot{p}_d$, where $K_p, K_v \in \mathbb{R}^{3\times 3}$ are user-selected positive-definite gain matrices. Projecting the desired force F_d to the body-fixed z-axis Re_3, we obtain the desired thrust f as the first control input:

$$f = -F_d \cdot (Re_3). \tag{2}$$

The desired thrust is used for controlling the translational motion of the quadrotor. For controlling the rotational motion, we use the moment M. We first define the desired rotation matrix R_d as follows. The desired z-axis is along the desired force, i.e., $b_{3d} = F_d/\|F_d\|$, where we assume that $\|F_d\| \neq 0$. Note that b_{3d} is the third column of R_d, and we compute the other two columns using an intermediate axis $b_{\text{int}} = [\cos\psi_d \ \sin\psi_d \ 0]^\top$ associated with the desired yaw ψ_d. The second and first column of the desired rotation matrix are $b_{2d} = b_{3d} \times b_{\text{int}}/\|b_{3d} \times b_{\text{int}}\|$ and $b_{1d} = b_{2d} \times b_{3d}$, respectively, where we assume $\|b_{3d} \times b_{\text{int}}\| \neq 0$. We now have $R_d = [b_{1d} \ b_{2d} \ b_{3d}]$. The attitude error is $e_R = (R_d^\top R - R^\top R_d)^\vee/2$, where $^\vee$ is the *vee* operator that takes elements of $\mathfrak{so}(3)$ to $\mathbb{R}^3$. The angular velocity error is $e_\Omega = \Omega - R^\top R_d \Omega_d$, and the desired moment is computed via

$$\begin{aligned} M = &-K_R e_R - K_\Omega e_\Omega + \Omega \times J\Omega \\ &- J(\Omega^\wedge R^\top R_d \Omega_d - R^\top R_d \dot{\Omega}_d), \end{aligned} \tag{3}$$

where $K_R, K_\Omega \in \mathbb{R}^{3\times 3}$ are user-selected positive-definite gain matrices. The derivation of Ω_d and $\dot{\Omega}_d$ are omitted in this paper for simplicity; see [40, Appendix F] for details.

To summarize, the geometric controller tracks the position p_d and yaw angle ψ_d by setting the thrust f and moment M via (2) and (3), respectively. For the stability proof of system (1) with the geometric controller (2) and (3), see [10, Prop. 3].

III. Geometric controller with $\mathcal{L}_1$ augmentation

The nominal dynamics (1) provide a description of a quadrotor's motion in an ideal case. However, in reality, a quadrotor's motion is affected by uncertainties and disturbances, such as propellers' aerodynamic effects, ground effect, and wind, for which establishing precise models is expensive with only marginal practical benefits. Next, we introduce the uncertainties to the state-space representation of the system.

Define state variable $x \in \mathbb{R}^{12}$ of the nominal dynamics (1) by $x^\top = [p^\top \ v^\top \ \phi \ \theta \ \psi \ \Omega^\top]$ and define the partial state $z \in \mathbb{R}^6$ by $z^\top = [v^\top \ \Omega^\top]$. The state-space form of (1b) and (1d) with partial state z is

$$\dot{z}(t) = f(z(t)) + B(R(t))u_b(t), \tag{4}$$

where $f(z) = \begin{bmatrix} ge_3 \\ -J^{-1}\Omega \times J\Omega \end{bmatrix}$, $B(R) = \begin{bmatrix} -m^{-1}Re_3 & 0_{3\times 3} \\ 0_{3\times 1} & J^{-1} \end{bmatrix}$, and $u_b^\top = [f \ M^\top]$ is the baseline (geometric) controller. The uncertainties enter the system (1) via (1b) and (1d), which results in the uncertain dynamics:

$$\begin{aligned} \dot{z}(t) = &f(z(t)) + B(R(t))(u_b(t) + \sigma_m(t, x(t))) \\ &+ B^\perp(R(t))\sigma_{um}(t, x(t)), \end{aligned} \tag{5}$$

where $\sigma_m \in \mathbb{R}^4$ and $\sigma_{um} \in \mathbb{R}^2$ stand for the matched and unmatched uncertainties, respectively, and $B^\perp(R) = \begin{bmatrix} m^{-1}Re_1 & m^{-1}Re_2 \\ 0_{3\times 1} & 0_{3\times 1} \end{bmatrix}$. The matched uncertainty σ_m enters the system in the same way as the control channel u_b (through $B(R)$) and, hence, can be compensated by the $\mathcal{L}_1$ adaptive controller, whereas the unmatched one σ_{um} enters the system through $B^\perp(R)$ whose columns are perpendicular to those of $B(R)$. A physical interpretation for uncertainties $\{\sigma_m, \sigma_{um}\}$ is the unmodelled force $F_0 \in \mathbb{R}^3$ and moment $M_0 \in \mathbb{R}^3$ applied to the COM in the body-fixed frame. In this case, the matched uncertainty σ_m contains F_0's projection onto the body-z axis and M_0 (i.e., $\sigma_m^\top = [F_0 \cdot Re_3 \ M_0^\top]$), whereas the unmatched uncertainty σ_{um} contains F_0's projection onto the body-xy plane (i.e., $\sigma_{um}^\top = [F_0 \cdot Re_1 \ F_0 \cdot Re_2]$. The uncertainties in (5) also apply to the case with perturbed mass and moment of inertia (see details in [37]). Note that we do not consider input constraints in this paper. For the readers who are interested in incorporating input saturation, please refer to [41].

Notice that both types of uncertainties, $\sigma_m(t, x(t))$ and $\sigma_{um}(t, x(t))$, are modelled as nonparametric uncertainties, i.e., they cannot be parameterized with a finite number of parameters (in the form of $\xi W(x)$ for ξ being unknown parameters and $W(x)$ being known vector-valued nonlinear functions of x) [42]. Another important feature is that both uncertainties are time- and state-dependent, which applies to a broad class of uncertainties in practice.

The $\mathcal{L}_1$ adaptive controller includes a state predictor, an adaptation law, and a low-pass filter (LPF) as shown in Fig. 2. The state predictor replicates the systems' structure, with the unknown uncertainties replaced by their estimates. If the uncertainty estimation by the adaptation law is accurate, then the prediction error should go to zero. The $\mathcal{L}_1$ control u_{ad}

is inserted to the uncertain dynamics such that

$$\dot{z}(t) = f(z(t)) + B(R(t))\,(u_b(t) + u_{ad}(t) + \sigma_m(t, x(t))) \\ + B^{\perp}(R(t))\sigma_{um}(t, x(t)), \quad (6)$$

where $u_{ad} \in \mathbb{R}^4$ such that $u_{ad}^\top = [u_{f_{\mathcal{L}_1}}^\top \; u_{M_{\mathcal{L}_1}}^\top]$. The state predictor is

$$\dot{\hat{z}}(t) = f(z(t)) + B(R(t))(u_b(t) + u_{ad}(t) + \hat{\sigma}_m(t)) \\ + B^{\perp}(R(t))\hat{\sigma}_{um}(t) + A_s\tilde{z}(t), \quad (7)$$

where $\tilde{z} = \hat{z} - z$ is the prediction error and $A_s \in \mathbb{R}^{6\times 6}$ is a user-selected diagonal Hurwitz matrix (which drives the prediction error $\|\tilde{z}\|$ to 0 exponentially fast). We use the piecewise-constant adaptation law such that for $t \in [iT_s, (i+1)T_s)$

$$\hat{\sigma}(t) = \hat{\sigma}(iT_s) = -\bar{B}(iT_s)^{-1}\Phi^{-1}\mu(iT_s), \quad (8)$$

where $\hat{\sigma}^\top = [\hat{\sigma}_m^\top \; \hat{\sigma}_{um}^\top]$, T_s is the time step, $\bar{B}(iT_s) = [B(R(iT_s)) \; B^{\perp}(R(iT_s))]$, $\Phi = A_s^{-1}(\exp(A_sT_s) - I)$, and $\mu(iT_s) = \exp(A_sT_s)\tilde{z}(iT_s)$ for $i \in \mathbb{N}$. Note that the square matrix $\bar{B}$ is invertible since it has full rank. Moreover, each element of $\bar{B}^{-1}$ has an explicit form, which enables fast computation of this matrix inverse.

The $\mathcal{L}_1$ control law only compensates for the matched uncertainty σ_m within the bandwidth of the LPF with transfer function $C(s)$:

$$u_{ad}(s) = -C(s)\hat{\sigma}_m(s), \quad (9)$$

where the signals are posed in the Laplacian domain and the filter bandwidth ω_c needs to satisfy the stability conditions [43, Sec. III].

The piecewise constant adaptation law can completely eliminate the state prediction error dynamics $\tilde{z}(iT_s)$ at the next sample time $(i+1)T_s$. To see how it works, consider the state prediction error via subtracting (6) from (7):

$$\dot{\tilde{z}}(t) = A_s\tilde{z}(t) + \bar{B}(t)(\hat{\sigma}(t) - \sigma(t)), \quad (10)$$

where $\sigma^\top = [\sigma_m^\top \; \sigma_{um}^\top]$. Without loss of generality, assume that the initial prediction error is nonzero, i.e., $\tilde{z}(0) \neq 0$. The closed-form solution for (10) is

$$\tilde{z}(T_s) = \exp(A_sT_s)\tilde{z}(0) + (\exp(A_sT_s) - I)\,A_s^{-1}\bar{B}(0)\hat{\sigma}(0) \\ + \int_0^{T_s} \exp((T_s - t)A_s)\bar{B}(0)\sigma(t)\mathrm{d}t \quad (11)$$

due to (10)'s linearity and $\bar{B}(t)$ and $\hat{\sigma}(t)$ being constants for $t \in [0, T_s)$. Setting $i = 0$ in (8) and plugging $\hat{\sigma}(0)$ in (11), the prediction error takes the form $\tilde{z}(T_s) = \int_0^{T_s} \exp((T_s - t)A_s)\bar{B}\sigma(t)\mathrm{d}t$, where the initial error $\tilde{z}(0)$ does not show up. Moreover, the error $\tilde{z}(T_s)$ will be eliminated in $\tilde{z}(2T_s)$ following the same logic. By setting the sampling time T_s small enough (up to the hardware limit), one can keep $\|\tilde{z}\|$ small and achieve arbitrary fast uncertainty compensation. Note that small T_s may result in high adaptation gain $\Phi^{-1}\exp(A_sT_s)$ in (8), which achieves fast estimation. Simultaneously, the high adaptation gain will introduce high-frequency components in the estimates. Therefore, we filter the uncertainty estimates to reject the high-frequency components from entering the control channel. Thus, the fast estimation is decoupled from the control channel and cannot hurt the robustness of the system.

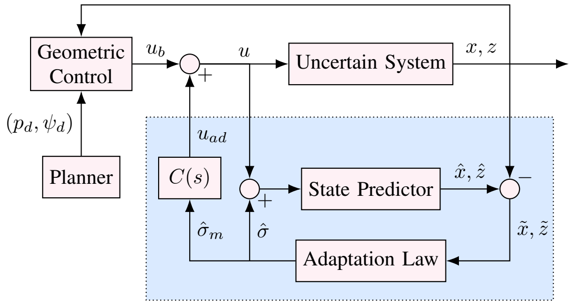

Fig. 2: The framework of geometric control with $\mathcal{L}_1$ augmentation, where the $\mathcal{L}_1$ controller is highlighted in blue.

Our design of the $\mathcal{L}_1$ controller is based on the partial state z instead of the full state x for the following two reasons. First, the kinematics (1a) and (1c) are uncertainty-free. Therefore, we only consider the partial state z that is directly affected by the uncertainties. Next, if we use the full state x, then the matrix $\bar{B} = [B(R) \; B^{\perp}(R)] \in \mathbb{R}^{12\times 6}$ is not square, which results in the infeasibility of (8) since $\bar{B}^{-1}$ is not well-defined. For complete proofs of stability and performance of $\mathcal{L}_1$ adaptive controller refer to [25].

IV. Experimental results

We demonstrate the proposed $\mathcal{L}_1$ augmentation on a Mambo quadrotor (displayed in Fig. 1) in experiments. We design our controller in Simulink and generate C code for the quadrotor's onboard execution [44]. All the computations including state estimation, baseline and $\mathcal{L}_1$ control calculation, and data logging run onboard at 200 Hz. For the LPF, we use a first-order LPF for the thrust channel and two cascaded first-order LPFs for the moment channel. The position of the quadrotor is provided from Vicon cameras at 120 Hz. We set $\Omega_d = \dot{\Omega}_d = 0$ for simplicity in implementation. A list of parameters in the experiments is shown in Table I.

A. Uncertainty estimation and compensation

We illustrate the $\mathcal{L}_1$ augmentation's capability of handling uncertainty by injecting signals to the control channel. The injected signals, denoted by σ_{inj}, serve as artificial uncertainties such that the total (matched) uncertainty is the sum of existing uncertainties in the system and the injected σ_{inj}.

TABLE I: Parameters in experiments.

param.	value	param.	value
m	0.075 kg	J	10^{-5}diag[5.8 7.2 10] kgm^2
g	9.81 m/s^2	K_p	10^{-1}diag[6.2 4.5 6.9]
T_s	0.005 s	K_v	10^{-1}diag[1 1 1.5]
ω_c (f)	8 rad/s	K_R	10^{-2}diag[1.5 1.5 0.2]
ω_c (M)	4, 6 rad/s	K_Ω	10^{-3}diag[2.2 2.2 0.7]
		A_s	$-$diag[5 5 5 10 10 10]

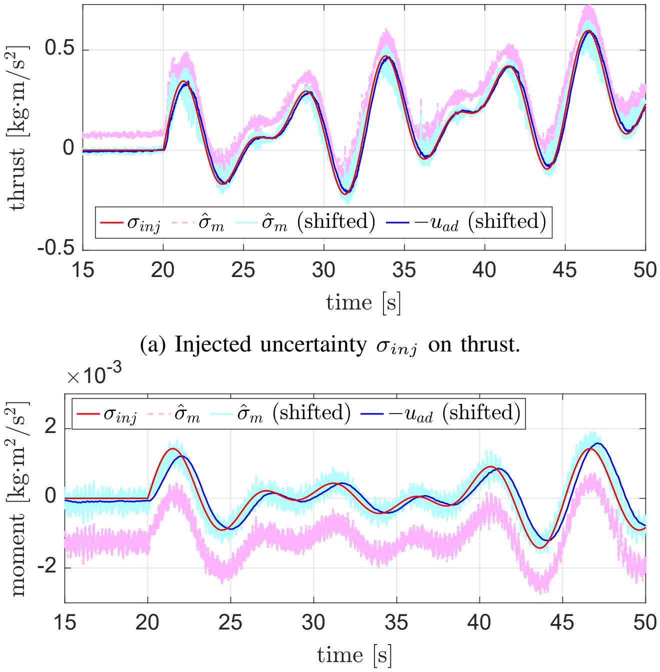

(a) Injected uncertainty σ_{inj} on thrust.

(b) Injected uncertainty σ_{inj} on pitch moment.

Fig. 3: $\mathcal{L}_1$ controller's uncertainty estimate $\hat{\sigma}_m$ and compensation $-u_{ad}$ versus the injected uncertainty σ_{inj}. We shift $\hat{\sigma}_m$ and $-u_{ad}$ vertically to show their convergence to σ_{inj}.

The uncertainty σ_m should be estimated by the adaptation law by $\hat{\sigma}_m$ and then compensated by the $\mathcal{L}_1$ controller. For illustration purposes, we set the first element of $\sigma_{\text{inj}}(t)$ to be $0.2\sin(t-20)+0.01(t-20)+0.15\sin(1.5(t-20))$ for $t \in [20, 50]$, and the other elements of $\sigma_{inj}(t)$ are set to 0 for the entire time. In other words, the injected uncertainty only applies to the thrust from 20 to 50 s. We set the quadrotor to hover at 1 m altitude so that the uncertainty estimate's convergence to the injected uncertainty can be clearly observed. The result is shown in Fig. 3a. The uncertainty estimate $\hat{\sigma}_m$ quickly converges to the injected signal σ_{inj}, and u_{ad} compensates for the injected uncertainty. Figure 3b shows similar uncertainty estimation and compensation results for the case when the injected uncertainty only applies to the third element of σ_m (pitch moment), where the injected signal is $10^{-3}(2\sin(t-20)+0.2(t-20)+\sin(0.75(t-20))$ for $t \in [20, 50]$. Note that the injected signals in this subsection, and later in Table II, have a significant impact to the quadrotor's linear acceleration $\dot{v}$ (angular acceleration $\dot{\Omega}$) since σ_{inj} is scaled by m^{-1} (J^{-1}).

B. Tracking performance

We compare the performance of the $\mathcal{L}_1$ augmentation to that of the baseline controller only. We deploy the controllers to track a "Figure 8" and a tilted "Figure 8"-shaped trajectory (shown in Fig. 4) in Experiments 1 and 2, respectively. In Experiment 1, we consider the following six cases:

1) no artificial uncertainty;
2) time-dependent uncertainty (see Table II);
3) state-dependent uncertainty (see Table II);

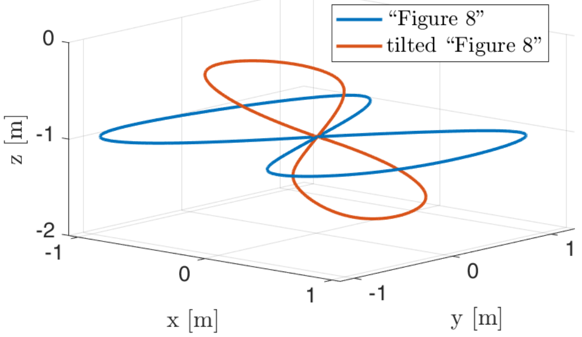

Fig. 4: Desired trajectories in Experiments 1 and 2.

4) unknown input gain $\beta(t) = 1+0.4\sin(t-5)$ on the pitch moment for $t \in [5, 22]$;
5) chipped propeller: propeller on motor 1 is cut off by 0.9 cm (14% of a propeller);
6) poorly tuned baseline controller.

The time- and state-dependent artificial uncertainties in Cases 2 and 3 are injected into the control channel. The unknown input gain β applies to the input matrix $B(R)$ such that the actual input to the system in (6) is multiplied by $\beta B(R)$, which associates with the scenario where the input matrix has time-varying model uncertainties. Tuning a nonlinear controller is a challenging task, which requires significant model knowledge and can be time consuming [45]. Case 6 is deliberately included to demonstrate that the $\mathcal{L}_1$ augmentation can achieve the same level of performance despite a poorly tuned baseline controller. In our case, the poorly tuned baseline controller uses smaller gains K_p and K_R than those in Table I, which results in significantly larger steady-state error and slower response to commands. Note that Cases 4 and 6 do not apply to the uncertainty model (5): we use them to empirically demonstrate the performance of $\mathcal{L}_1$ augmentation.

The root-mean-square error (RMSE) for trajectory tracking is shown in Fig. 5a. The $\mathcal{L}_1$ augmentation can maintain a consistent and much smaller RMSE tracking error compared to that of the baseline controller alone under various types of uncertainties.

In Experiment 2, we consider the same cases as in Experiment 1 except:

2) mixed uncertainties (see Table II) with unknown input gain $\beta(t) = 1+0.2\sin(t-5)$ on the thrust for $t \in [5, 22]$;
3) unknown input gain $\beta(t) = 1+0.2\sin(t-5)$ on the thrust for $t \in [5, 22]$;

The RMSE for trajectory tracking is shown in Fig 5b. The $\mathcal{L}_1$ augmentation can maintain a relatively small and consistent RMSE on trajectory tracking, whereas the performance of the baseline controller alone suffers from uncertainties. Note that for the case with state-dependent uncertainty, the baseline controller alone crashed the quadrotor in all trials, whereas the case with the $\mathcal{L}_1$ augmentation can stabilize the quadrotor and maintain a good tracking performance.

We add different slung weights to the quadrotor during hover and compare the position-holding performance be-

TABLE II: List of injected uncertainties in Experiments 1 and 2 for time $t \in [5, 22]$.

Exp.	Case	σ_m (thrust)	σ_m (roll moment)	σ_m (pitch moment)
1	2	0	$0.001\sin(0.75(t-5))$	$0.0008\sin(t-5)+0.0008\sin(0.5(t-5))$
1	3	0	$0.001\sin(0.75(t-5))$	$0.0005\sin(t-5)p_1^2(t)$
2	2	0	$0.001\sin(0.75(t-5))$	$0.01\sin(t-5)p_1^2(t)$
2	3	$0.2\sin(0.5(t-5))+0.15\sin(0.75(t-5))$	$0.001\sin(0.75(t-5))$	$0.0008(\sin(t-5)+\sin(0.5(t-5)))$

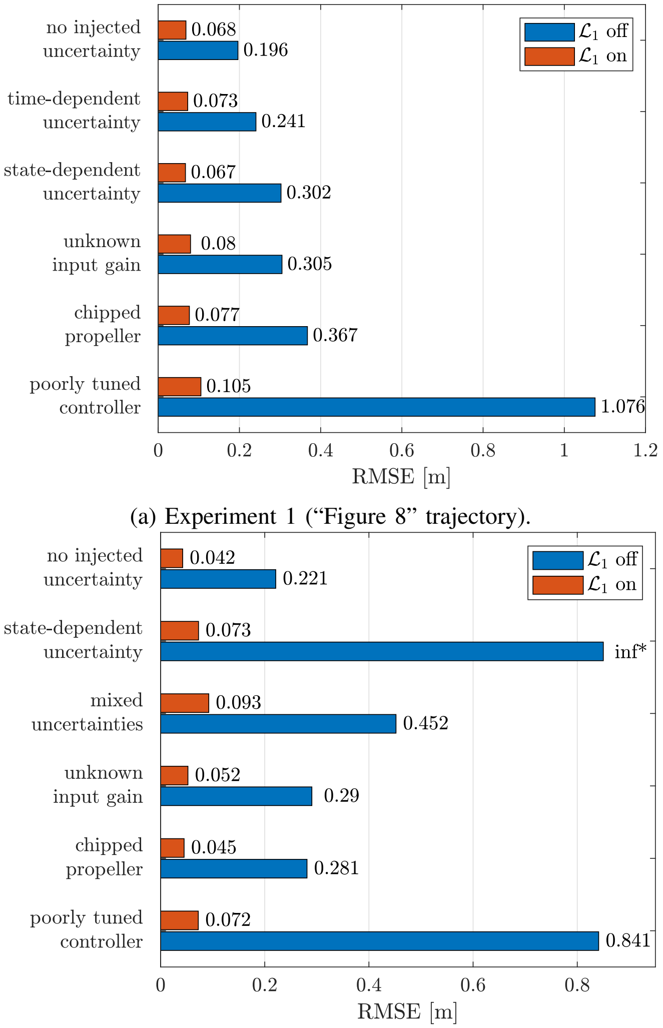

(a) Experiment 1 ("Figure 8" trajectory).

(b) Experiment 2 (tilted "Figure 8" trajectory). The "inf*" mark refers to the failed trial using the baseline controller alone under state-dependent uncertainty.

Fig. 5: Comparisons of tracking error under various types of uncertainties between the baseline controller alone ($\mathcal{L}_1$ off) and the baseline controller with $\mathcal{L}_1$ augmentation ($\mathcal{L}_1$ on).

tween the $\mathcal{L}_1$ augmentation and the baseline controller alone. Figure 6 shows the tracking errors. The $\mathcal{L}_1$ augmentation quickly adapts to the added weights and corrects the position errors, whereas the baseline controller can barely hold its position.

It worth noting that the $\mathcal{L}_1$ controller uses the same set of parameters in all cases and in all experiments (the baseline controller uses the parameters in Table I for Cases 1–5). The relatively small and consistent tracking errors with the $\mathcal{L}_1$ augmentation shown in Fig. 5 demonstrate the superior performance and ease of use of the $\mathcal{L}_1$ controller under various types of uncertainties and for different trajectories without any redesign or retuning. Furthermore, when tracking trajectories, our approach handles the uncertainties by design, which does not require data collection and (neural network) training that are typically used in ML-based approaches, e.g., [21], [23].

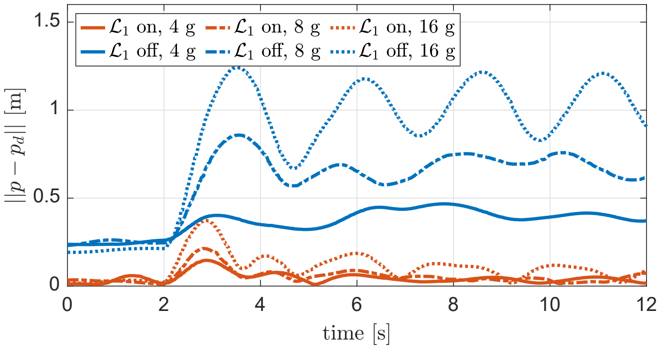

Fig. 6: Comparison of tracking errors for hovering in the cases with and without $\mathcal{L}_1$ augmentation under added slung weights. The weights are added at 2 s. The 4/8/16 g weights correspond to 5.3/10.7/21.3% of the quadrotor's weight.

V. Conclusion

In this paper, we develop, test, and validate an $\mathcal{L}_1$ adaptive controller design for a quadrotor to track a prescribed trajectory. An $\mathcal{L}_1$ augmentation of a baseline geometric controller is formulated, where the latter stabilizes the quadrotor on $SE(3)$ and the former compensates for the uncertainties and disturbances acting on the system. The $\mathcal{L}_1$ controller is based on the quadrotor's partial state that is directly affected by the uncertainties, which allows using a piecewise-constant adaptation law for uncertainty estimation. Experimental results on a Mambo quadrotor show that the uncertainty estimate quickly converges to the uncertainty, and the matched uncertainty is completely compensated for upon estimation. The $\mathcal{L}_1$ augmentation also demonstrates consistent and smaller (five times smaller on average) trajectory tracking errors compared with the baseline controller alone for different target trajectories and under various types of uncertainties.

Future work includes modifying the current design to attenuate the unmatched uncertainties [46] and applying learning techniques (e.g., [47]) to better characterize the uncertainties using data. Learned information could be incorporated in the proposed control framework, which alleviates workloads for $\mathcal{L}_1$ adaptive controller and achieves better performance without sacrificing the robustness of the system.

REFERENCES

[1] H. C. Yang, R. AbouSleiman, B. Sababha, E. Gjioni, D. Korff, and O. Rawashdeh, "Implementation of an autonomous surveillance quadrotor system," in *Proceedings of AIAA Infotech@Aerospace Conference*, Seattle, WA, USA, 2009, p. 2047.

[2] Y. Tian, K. Liu, K. Ok, L. Tran, D. Allen, N. Roy, and J. P. How, "Search and rescue under the forest canopy using multiple UAVs," *The International Journal of Robotics Research*, vol. 39, no. 10-11, pp. 1201–1221, 2020.

[3] J. Valente, D. Sanz, J. Del Cerro, A. Barrientos, and M. Á. de Frutos, "Near-optimal coverage trajectories for image mosaicing using a mini quad-rotor over irregular-shaped fields," *Precision Agriculture*, vol. 14, no. 1, pp. 115–132, 2013.

[4] D. Mellinger, M. Shomin, N. Michael, and V. Kumar, "Cooperative grasping and transport using multiple quadrotors," in *Distributed Autonomous Robotic Systems*. Berlin, Germany: Springer, 2013, pp. 545–558.

[5] D. Mellinger, N. Michael, and V. Kumar, "Trajectory generation and control for precise aggressive maneuvers with quadrotors," *The International Journal of Robotics Research*, vol. 31, no. 5, pp. 664–674, 2012.

[6] A. Tayebi and S. McGilvray, "Attitude stabilization of a VTOL quadrotor aircraft," *IEEE Transactions on Control Systems Technology*, vol. 14, no. 3, pp. 562–571, 2006.

[7] S. P. Bhat and D. S. Bernstein, "A topological obstruction to continuous global stabilization of rotational motion and the unwinding phenomenon," *Systems & Control Letters*, vol. 39, no. 1, pp. 63–70, 2000.

[8] C. G. Mayhew, R. G. Sanfelice, and A. R. Teel, "Quaternion-based hybrid control for robust global attitude tracking," *IEEE Transactions on Automatic Control*, vol. 56, no. 11, pp. 2555–2566, 2011.

[9] D. Mellinger and V. Kumar, "Minimum snap trajectory generation and control for quadrotors," in *Proceedings of IEEE International Conference on Robotics and Automation*, Shanghai, China, 2011, pp. 2520–2525.

[10] T. Lee, M. Leok, and N. H. McClamroch, "Geometric tracking control of a quadrotor UAV on SE(3)," in *Proceedings of the 49th IEEE Conference on Decision and Control*, Atlanta, GA, USA, 2010, pp. 5420–5425.

[11] B. J. Emran and H. Najjaran, "A review of quadrotor: An underactuated mechanical system," *Annual Reviews in Control*, vol. 46, pp. 165–180, 2018.

[12] Z. T. Dydek, A. M. Annaswamy, and E. Lavretsky, "Adaptive control of quadrotor UAVs: A design trade study with flight evaluations," *IEEE Transactions on Control Systems Technology*, vol. 21, no. 4, pp. 1400–1406, 2012.

[13] J. M. Selfridge and G. Tao, "A multivariable adaptive controller for a quadrotor with guaranteed matching conditions," *Systems Science & Control Engineering*, vol. 2, no. 1, pp. 24–33, 2014.

[14] G. Antonelli, E. Cataldi, F. Arrichiello, P. R. Giordano, S. Chiaverini, and A. Franchi, "Adaptive trajectory tracking for quadrotor MAVs in presence of parameter uncertainties and external disturbances," *IEEE Transactions on Control Systems Technology*, vol. 26, no. 1, pp. 248–254, 2017.

[15] D. Cabecinhas, R. Cunha, and C. Silvestre, "A nonlinear quadrotor trajectory tracking controller with disturbance rejection," *Control Engineering Practice*, vol. 26, pp. 1–10, 2014.

[16] S. Bouabdallah and R. Siegwart, "Backstepping and sliding-mode techniques applied to an indoor micro quadrotor," in *Proceedings of IEEE International Conference on Robotics and Automation*. Barcelona, Spain: IEEE, 2005, pp. 2247–2252.

[17] M. Labbadi and M. Cherkaoui, "Robust adaptive backstepping fast terminal sliding mode controller for uncertain quadrotor UAV," *Aerospace Science and Technology*, vol. 93, p. 105306, 2019.

[18] N. Ahmed, M. Chen, and S. Shao, "Disturbance observer based tracking control of quadrotor with high-order disturbances," *IEEE Access*, vol. 8, pp. 8300–8313, 2020.

[19] A. Castillo, R. Sanz, P. Garcia, W. Qiu, H. Wang, and C. Xu, "Disturbance observer-based quadrotor attitude tracking control for aggressive maneuvers," *Control Engineering Practice*, vol. 82, pp. 14–23, 2019.

[20] F. A. Goodarzi, D. Lee, and T. Lee, "Geometric adaptive tracking control of a quadrotor unmanned aerial vehicle on SE(3) for agile maneuvers," *Journal of Dynamic Systems, Measurement, and Control*, vol. 137, no. 9, p. 091007, 2015.

[21] G. Shi, W. Hönig, Y. Yue, and S.-J. Chung, "Neural-swarm: Decentralized close-proximity multirotor control using learned interactions," in *Proceedings of IEEE International Conference on Robotics and Automation*. Virtual Conference: IEEE, 2020, pp. 3241–3247.

[22] P. Bouffard, A. Aswani, and C. Tomlin, "Learning-based model predictive control on a quadrotor: Onboard implementation and experimental results," in *Proceedings of IEEE International Conference on Robotics and Automation*. Saint Paul, Minnesota, USA: IEEE, 2012, pp. 279–284.

[23] G. Torrente, E. Kaufmann, P. Föhn, and D. Scaramuzza, "Data-driven MPC for quadrotors," *IEEE Robotics and Automation Letters*, vol. 6, no. 2, pp. 3769–3776, 2021.

[24] G. Joshi, J. Virdi, and G. Chowdhary, "Asynchronous deep model reference adaptive control," *arXiv:2011.02920*, 2020, accepted for publication in Conference on Robots Learning 2020.

[25] N. Hovakimyan and C. Cao, *$\mathcal{L}_1$ Adaptive Control Theory: Guaranteed Robustness with Fast Adaptation*. Philadelphia, PA, USA: SIAM, 2010.

[26] I. Gregory, C. Cao, E. Xargay, N. Hovakimyan, and X. Zou, "$\mathcal{L}_1$ adaptive control design for NASA AirSTAR flight test vehicle," in *Proceedings of AIAA Guidance, Navigation, and Control Conference*, Chicago, IL, USA, 2009, p. 5738.

[27] I. Gregory, E. Xargay, C. Cao, and N. Hovakimyan, "Flight test of an $\mathcal{L}_1$ adaptive controller on the NASA AirSTAR flight test vehicle," in *Proceedings of AIAA Guidance, Navigation, and Control Conference*, Toronto, Ontario, Canada, 2010, p. 8015.

[28] K. Ackerman, E. Xargay, R. Choe, N. Hovakimyan, M. C. Cotting, R. B. Jeffrey, M. P. Blackstun, T. P. Fulkerson, T. R. Lau, and S. S. Stephens, "$\mathcal{L}_1$ stability augmentation system for Calspan's variable-stability Learjet," in *Proceedings of AIAA Guidance, Navigation, and Control Conference*, San Diego, CA, USA, 2016, p. 0631.

[29] K. A. Ackerman, E. Xargay, R. Choe, N. Hovakimyan, M. C. Cotting, R. B. Jeffrey, M. P. Blackstun, T. P. Fulkerson, T. R. Lau, and S. S. Stephens, "Evaluation of an $\mathcal{L}_1$ adaptive flight control law on Calspan's Variable-Stability Learjet," *AIAA Journal of Guidance, Control, and Dynamics*, vol. 40, no. 4, pp. 1051–1060, 2017.

[30] I. Kaminer, A. Pascoal, E. Xargay, N. Hovakimyan, C. Cao, and V. Dobrokhodov, "Path following for small unmanned aerial vehicles using $\mathcal{L}_1$ adaptive augmentation of commercial autopilots," *AIAA Journal of Guidance, Control, and Dynamics*, vol. 33, no. 2, pp. 550–564, 2010.

[31] I. Kaminer, E. Xargay, V. Cichella, N. Hovakimyan, A. M. Pascoal, A. P. Aguiar, V. Dobrokhodov, and R. Ghabcheloo, "Time-critical cooperative path following of multiple UAVs: Case studies," in *Itzhack Y. Bar-Itzhack Memorial Symposium on Estimation, Navigation, and Spacecraft Control*. Berlin, Germany: Springer, 2012, pp. 209–233.

[32] H. Jafarnejadsani, D. Sun, H. Lee, and N. Hovakimyan, "Optimized $\mathcal{L}_1$ adaptive controller for trajectory tracking of an indoor quadrotor," *Journal of Guidance, Control, and Dynamics*, vol. 40, no. 6, pp. 1415–1427, 2017.

[33] Z. Zuo and P. Ru, "Augmented $\mathcal{L}_1$ adaptive tracking control of quad-rotor unmanned aircrafts," *IEEE Transactions on Aerospace and Electronic Systems*, vol. 50, no. 4, pp. 3090–3101, 2014.

[34] M. Q. Huynh, W. Zhao, and L. Xie, "$\mathcal{L}_1$ adaptive control for quadcopter: Design and implementation," in *Proceedings of the 13th International Conference on Control Automation Robotics & Vision*. Singapore: IEEE, 2014, pp. 1496–1501.

[35] P. Kotaru, R. Edmonson, and K. Sreenath, "Geometric $\mathcal{L}_1$ adaptive attitude control for a quadrotor unmanned aerial vehicle," *Journal of Dynamic Systems, Measurement, and Control*, vol. 142, no. 3, p. 031003, 2020.

[36] P. A. Ioannou, A. M. Annaswamy, K. S. Narendra, S. Jafari, L. Rudd, R. Ortega, and J. Boskovic, "$\mathcal{L}_1$-adaptive control: Stability, robustness, and interpretations," *IEEE Transactions on Automatic Control*, vol. 59, no. 11, pp. 3075–3080, 2014.

[37] J. Pravitra, K. A. Ackerman, C. Cao, N. Hovakimyan, and E. A. Theodorou, "$\mathcal{L}_1$-Adaptive MPPI Architecture for Robust and Agile Control of Multirotors," in *Proceedings of IEEE/RSJ International Conference on Intelligent Robots and Systems*. Las Vegas, NV, USA: IEEE, 2020, pp. 7661–7666.

[38] J. Diebel, "Representing attitude: Euler angles, unit quaternions, and rotation vectors," *Matrix*, vol. 58, no. 15-16, pp. 1–35, 2006.

[39] M. J. Van Nieuwstadt and R. M. Murray, "Real-time trajectory generation for differentially flat systems," *International Journal of Robust and Nonlinear Control*, vol. 8, no. 11, pp. 995–1020, 1998.

[40] T. Lee, M. Leok, and N. H. McClamroch, “Control of complex maneuvers for quadrotor UAV using geometric methos on SE (3),” *arXiv:1003.2005*, 2010.

[41] D. Li, N. Hovakimyan, and C. Cao, “$\mathcal{L}_1$ adaptive controller in the presence of input saturation,” in *Proceedings of AIAA Guidance, Navigation, and Control Conference*, Chicago, IL, USA, 2009, p. 6064.

[42] S. Boyd, “A note on parametric and nonparametric uncertainties in control systems,” in *Proceedings of American Control Conference*. Seattle, WA, USA: IEEE, 1986, pp. 1847–1849.

[43] A. Lakshmanan, A. Gahlawat, and N. Hovakimyan, “Safe feedback motion planning: A contraction theory and $\mathcal{L}_1$-adaptive control based approach,” in *Proceedings of the 59th IEEE Conference on Decision and Control*. Jeju, Korea: IEEE, 2020, pp. 1578–1583.

[44] MathWorks. Simulink Support Package for Parrot Minidrones. [Online]. Available: https://www.mathworks.com/help/supportpkg/parrot/

[45] F. Berkenkamp, A. P. Schoellig, and A. Krause, “Safe controller optimization for quadrotors with Gaussian processes,” in *Proceedings of IEEE International Conference on Robotics and Automation*. Stockholm, Sweden: IEEE, 2016, pp. 491–496.

[46] P. Zhao, S. Snyder, N. Hovakimyana, and C. Cao, “Robust adaptive control of linear parameter-varying systems with unmatched uncertainties,” *arXiv:2010.04600*, 2021.

[47] A. Gahlawat, A. Lakshmanan, L. Song, A. Patterson, Z. Wu, N. Hovakimyan, and E. A. Theodorou, “Contraction $\mathcal{L}_1$-adaptive control using Gaussian processes,” in *Proceedings of the 3rd Learning for Dynamics & Control*. Virtual Conference: PMLR, 2021, pp. 1027–1040.